

Modeling pO₂ Distributions in the Bone Marrow Hematopoietic Compartment. I. Krogh's Model

Dominic C. Chow, Larissa A. Wenning, William M. Miller, and E. Terry Papoutsakis

Department of Chemical Engineering, Northwestern University, Evanston, Illinois 60208-3120 USA

ABSTRACT Human bone marrow (BM) is a tissue of complex architectural organization, which includes granulopoietic loci, erythroblastic islets, and lymphocytic nodules. Oxygen tension (pO₂) is an important determinant of hematopoietic stem and progenitor cell proliferation and differentiation. Thus, understanding the impact of the BM architectural organization on pO₂ levels in extravascular hematopoietic tissue is an important biophysical problem. However, currently it is impossible to measure pO₂ levels and their spatial variations in the BM. Homogeneous Kroghian models were used to estimate pO₂ distribution in the BM hematopoietic compartment (BMHC) and to conservatively simulate pO₂-limited cellular architectures. Based on biophysical data of hematopoietic cells and characteristics of BM physiology, we constructed a tissue cylinder solely occupied by granulocytic progenitors (the most metabolically active stage of the most abundant cell type) to provide a physiologically relevant limiting case. Although the number of possible cellular architectures is large, all simulated pO₂ profiles fall between two extreme cases: those of homogeneous tissues with adipocytes and granulocytic progenitors, respectively. This was illustrated by results obtained from a parametric criterion derived for pO₂ depletion in the extravascular tissue. Modeling results suggest that stem and progenitor cells experience a low pO₂ environment in the BMHC.

NOMENCLATURE

K	= oxygen permeability (mol/cm/s/mm Hg),
K_M	= Michaelis-Menten constant (mm Hg)
N	= number of cell layers
N_{\max}	= maximum number of cell layers
P	= oxygen partial pressure (tension) (mm Hg)
P^*	= reduced oxygen tension
P_S	= saturation oxygen tension (mm Hg)
q_{O_2}	= specific oxygen uptake rate (mol/cell/h)
$Q(P)$	= volumetric oxygen consumption rate as a function of P (mol/cm ³ /s)
Q_{\max}	= maximum volumetric oxygen consumption rate (mol/cm ³ /s)
r	= distance from the center of the tissue cylinder (μm)
r^*	= reduced distance from the center of the tissue cylinder
R_1	= sinus radius (μm)
R_2	= tissue cylinder radius (μm)
$R_{2\max}$	= maximum tissue cylinder radius (μm)
\bar{V}	= specific cell volume (cm ³ /cell)

Greek symbols

β	= ratio of sinus radius to tissue cylinder radius
β_{\min}	= minimum ratio of sinus radius to tissue cylinder radius
ϕ	= Thiele modulus
ϕ'	= modified Thiele modulus
κ	= ratio of saturation oxygen tension to Michaelis-Menten constant

INTRODUCTION

Variations in oxygen concentration (or oxygen partial pressure, pO₂) in different tissues have both physiological and pathophysiological implications (Brizel et al., 1999; Carmeliet and Jain, 2000; Hansen-Algenstaedt et al., 2000; Leunig et al., 1992; Roh et al., 1991; Vaupel and Hoeckel, 1999). Oxygen tension distribution in a wide range of tissues has been both measured and modeled extensively in the context of understanding the physiological function of a tissue and associated pathophysiology. Oxygen tension is an important determinant of proliferation and differentiation of hematopoietic cells. Reduced oxygen tension (pO₂ = 38 mm Hg, 5% O₂) has been shown to enhance the production of erythroid, megakaryocytic, and granulocytic-monocytic progenitors in vitro (Bradley et al., 1978; Katahira and Mizoguchi, 1987; Koller et al., 1992; LaIuppa et al., 1998). The formation of mature erythrocytes and megakaryocytes is more extensive under a pO₂ value of 152 mm Hg (20% O₂) (LaIuppa et al., 1998; Mostafa et al., 2000), which is in contrast to greater production of differentiated granulocytes under 5% O₂ (Hevehan et al., 2000). These results are consistent with findings that progenitor cells of most hematopoietic lineages proliferate more rapidly in the regions farther away from the sinuses, and that mature erythrocytes

Received for publication 8 December 2000 and in final form 24 April 2001.

Address reprint requests to E. Terry Papoutsakis, Dept. Chemical Engineering, Northwestern University, 2145 Sheridan Road E136, Evanston, IL 60208-3120. Tel.: 847-491-7398; Fax: 847-491-3728; E-mail: e-paps@nwu.edu.

Dr. Wenning's present address: Department of Drug Metabolism, Merck Research Laboratories, West Point, PA 19486.

© 2001 by the Biophysical Society

0006-3495/01/08/675/10 \$2.00

and megakaryocytes are found primarily in the proximity of the sinuses, while granulocytes mature away from the sinuses (Weiss, 1991). It is important to understand the possible variations of pO_2 in the bone marrow hematopoietic compartment (BMHC) (the extravascular space for blood cell production) and how these variations might be affected by the various possible cellular arrangements (referred to as "architectures" in this and the companion paper).

Despite the crucial role played by oxygen in the proliferation and differentiation of hematopoietic cells, reported pO_2 measurements in the BMHC remain very limited. The reported mean pO_2 in the BM is ~ 52 mm Hg (Ishikawa and Ito, 1988), which is similar to the average pO_2 values of other normal tissues. However, there have been no spatial pO_2 measurements in the BMHC. Unlike other tissues (Helmlinger et al., 1997), direct *in vivo* measurements of pO_2 spatial variations in the BMHC are at present practically impossible. Thus, detailed modeling is the only available means to provide such estimates.

Krogh's model (Krogh, 1918), whereby the tissue is approximated by a cylinder with a single capillary at its center, has been well established and extensively used in modeling oxygen transfer through different types of tissues, including skeletal muscle (Krogh, 1919; Thews, 1960), myocardium (Grunewald and Sowa, 1978; Hoofd et al., 1987; Rakusan, 1971; Rakusan et al., 1984), brain (Ivanov et al., 1979; Reneau et al., 1967), lung (Weibel, 1984), and skin (Grossmann, 1982). Compared to other tissues, mathematical modeling of pO_2 distribution in the BMHC is more challenging due to the presence of multiple cell types and the complexity of cellular architectures. The diversity of hematopoietic cell types in the BM is reflected in their cellular compositions, sizes, and functions, which in turn affect oxygen consumption and transport properties. Therefore, the estimation of biophysical parameters is particularly important in obtaining reliable estimates from any biophysical-transport models.

Physically supported by vascular structures and stromal cells (such as adventitial reticular cells and endothelial cells), totipotent stem cells proliferate and differentiate to form less primitive pluripotent stem cells, which are the precursors of more differentiated cells of the myeloid and lymphoid lineages (Lichtman, 1984). Hematopoietic stem cells appear at a very low frequency in the BM, and the number of progenitor cells increases with the stage of maturation. From micrographs of the BMHC, as few as 4 to 8 to as many as 16 to 20 cells can be found tightly packed between two sinuses (Erslev and Weiss, 1983; Lichtman, 1984; Weiss, 1976). Therefore, many hematopoietic cells are 2 to 10 cell diameters away from the closest sinus. These cells are usually arranged in an organized fashion in the BMHC (Adler, 1984; Lichtman, 1984; Tavassoli and Yoffey, 1983; Weiss, 1991; Wickramasinghe, 1975):

1. The most primitive stem and progenitor cells, residing in the regions most distant from the sinus, move closer to the sinus lining as they differentiate, with the exception of granulocytes (in granulocytic loci), which may mature far from the sinuses (Weiss, 1991);
2. Mature erythrocytes occupy the perivascular space next to the adventitial surface, while immature erythrocytes (in erythroblastic islets made up of one to two macrophages surrounded by several layers of erythroid progenitors and mature erythrocytes; ~ 160 μm in diameter with the outermost erythroid-cell layer attached to one or more sinuses) are located mostly away from the sinus (Weiss, 1991);
3. Lymphocytes are organized in lymphocyte nodules (80–1200 μm in diameter) between two neighboring sinuses (Weiss, 1991);
4. Mature megakaryocytes, which may release platelets directly into circulation through gaps in the sinusoid wall, are always located next to the sinuses (Wickramasinghe, 1975);
5. Adipocytes usually reside in areas around sinuses at the center of the bone (yellow marrow), whereas red marrow (i.e., adipocyte-poor) is mostly localized near the bone endosteum (Marshall and Lichtman, 1981).

The objective of this study is to provide an estimate of the pO_2 distribution in BMHC and to determine the cellular architectures that produce the lowest pO_2 values. We simulated pO_2 distribution in the BMHC by constructing a tissue cylinder with a bone marrow sinus at its center, surrounded by different types of hematopoietic cells. In this first part of a two-part series we provide estimates for model parameters for various hematopoietic cell types and then simulate likely oxygen-limited cellular arrangements, in which the whole extravascular tissue is composed of one cell type. By using the homogeneous Kroghian model we develop a mathematical criterion for the occurrence of oxygen depletion and examine which cell types would produce the lowest pO_2 values. In the second part of this series we explore different types of more complex non-homogeneous biophysical-transport models to determine the effects of the BM cellular architecture (made up of different cell types) on the pO_2 distribution, and compare the results with estimates developed in the limiting cases of the present homogeneous Kroghian model.

MATHEMATICAL MODEL

As in other Kroghian models, the following assumptions are made to simplify mathematical formulation: 1) only steady-state oxygen transfer is considered; 2) oxygen molecules do not bind with any carriers or preferentially absorb on certain parts of the cells; 3) the sinuses are assumed to be straight and parallel for a length sufficient to establish equilibrium between the sinus and hematopoietic tissue; 4) oxygen

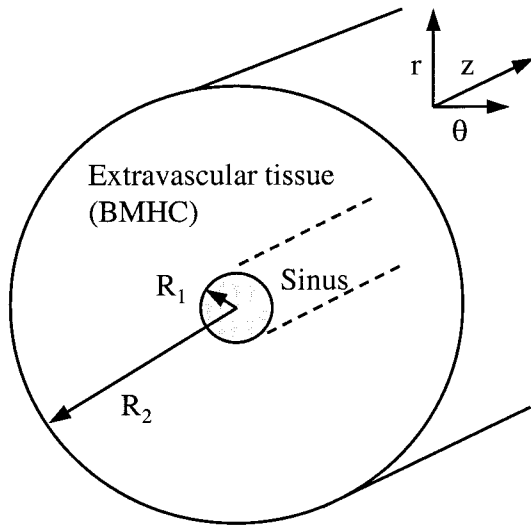


FIGURE 1 Graphical representation of the Kroghian model.

consumption and resistance to oxygen diffusion of the trilaminar sinusoidal wall are assumed to be insignificant.

Oxygen transport and utilization can be mathematically described as follows:

$$K\nabla^2 P = Q(P) \quad (1)$$

where K is the effective oxygen permeability (mol/cm/s/mm Hg), P is the oxygen partial pressure pO₂ (mm Hg), and $Q(P)$ is the volumetric oxygen consumption rate (mol/cm³/s). K is the product of the oxygen diffusivity (D , cm²/s) and the oxygen solubility coefficient (α , mol/cm³/mm Hg). Q is the ratio of the specific oxygen uptake rate (q_{O_2} , mol/cell/h) and the specific cell volume (\bar{V} , cm³/cell).

Assuming that P in the extravascular tissue depends only on the radial position (r) relative to the sinus, the oxygen continuity equation becomes

$$\frac{1}{r} \left[\frac{d}{dr} \left(r \frac{dP}{dr} \right) \right] = \frac{Q(P)}{K} \quad (2)$$

We assume that P at the sinus wall (R_1) equals the saturation oxygen tension (P_s) and that oxygen flux is zero when it reaches the boundary of the tissue cylinder (R_2) (symmetry boundary condition). Thus, we write the following two boundary conditions (Fig. 1).

$$P = P_s \quad \text{when} \quad r = R_1 \quad (\text{at the sinus wall}) \quad (3)$$

$$\frac{dP}{dr} = 0 \quad (4)$$

when

$$r = R_2 \quad (\text{at the outer boundary of the tissue cylinder})$$

A dimensionless form of the boundary-value problem is necessary to minimize the number of cases that must be simulated. We choose the tissue cylinder radius R_2 as the characteristic length and the saturation oxygen partial pressure P_s as the characteristic oxygen tension. We thus define:

$$P^* \equiv P/P_s \quad (\text{dimensionless partial pressure}) \quad (5)$$

$$r^* \equiv r/R_2 \quad (\text{dimensionless radius}) \quad (6)$$

$$R_1^* \equiv R_1/R_2 = \beta \quad (\text{dimensionless sinus radius}) \quad (7)$$

$$R_2^* \equiv R_2/R_2 = 1 \quad (\text{dimensionless tissue cylinder radius}) \quad (8)$$

By multiplying both sides of Eq. 2 by R_2^2/P_s we get

$$\frac{1}{r^*} \frac{d}{dr^*} \left(r^* \frac{dP^*}{dr^*} \right) = \frac{Q(P)}{K} \frac{R_2^2}{P_s} \quad (9)$$

The dimensionless boundary conditions are

$$P^* = 1 \quad \text{when} \quad r^* = \beta \quad (\text{at the sinus wall}) \quad (10)$$

$$\frac{dP^*}{dr^*} = 0 \quad (11)$$

when

$$r^* = 1 \quad (\text{at the outer boundary of the tissue cylinder})$$

The dependence of $Q(P)$ on oxygen tension can take three different forms: 1) zero-order kinetics,

$$Q(P) = Q_{\max} \quad (12)$$

where Q_{\max} is the maximal oxygen consumption rate; 2) first-order oxygen uptake kinetics,

$$Q(P) = k \cdot Q_{\max} \cdot P \quad (13)$$

where k is a constant with units of mm Hg⁻¹; and 3) saturation-type (Michaelis-Menten) oxygen uptake kinetics,

$$Q(P) = \frac{Q_{\max} P}{K_M + P} \quad (14)$$

where K_M is the oxygen affinity constant.

For simplicity, we will consider only zero-order kinetics for the oxygen consumption rate because oxygen profiles obtained using different kinetics deviate <5% from the estimates using the zero-order kinetics (data

TABLE 1 Summary of system and cellular parameters and model outputs

Symbol	Definition	Units
System		
R_1	Radius of the sinus	μm
R_2	Radius of the tissue cylinder	μm
N	Number of layers of different cell types	—
P_s	Saturated oxygen tension	mm Hg
Cellular		
q_{O_2}	Specific oxygen uptake rate	mol/cell/h
V	Specific cell volume	cm^3/cell
Q	Volumetric oxygen consumption rate	$\text{mol}/\text{cm}^3/\text{s}$
K	Effective permeability	$\text{mol}/\text{cm}/\text{s}/\text{mm Hg}$
K_M	Michaelis-Menten or oxygen affinity constant	mm Hg
Model Output		
P^*	Reduced oxygen tension	—
P_{R2}^*	P^* at the rim of the tissue cylinder	—
$R_{2\text{max}}$	Maximum tissue cylinder radius (for $P_{R2}^* \geq 0$)	μm
N_{max}	Maximum number of cell layers (for $P_{R2}^* \geq 0$)	—

not shown). In the case of zero-order kinetics, Eq. 2 becomes

$$\frac{1}{r^*} \frac{d}{dr^*} \left(r^* \frac{dP^*}{dr^*} \right) = \frac{Q_{\text{max}}}{K} \frac{R_2^2}{P_s} = \phi^2 \quad (15)$$

where the Thiele modulus

$$\phi \equiv R_2 \sqrt{\frac{Q_{\text{max}}}{K \cdot P_s}} \quad (16)$$

The solution to the dimensionless boundary value problem is

$$P^* = 1 + \phi^2 \left[\frac{r^{*2} - \beta^2}{4} + \frac{1}{2} \ln \left(\frac{\beta}{r^*} \right) \right] \quad (17)$$

This expression is known as the Krogh-Erlang equation (Krogh, 1919).

Because the number of possible cellular architectures in the BMHC is very large, it is not practical to individually simulate each of them to examine situations of low pO_2 or oxygen depletion. We can, however, develop a mathematical criterion for oxygen depletion from Eq. 17. Oxygen depletion occurs when pO_2 at the boundary of the tissue cylinder becomes zero, that is, when (using Eq. 17)

$$1 + \phi^2 \left[\frac{1^2 - \beta_{\text{min}}^2}{4} + \frac{1}{2} \ln \beta_{\text{min}} \right] = 0 \quad (18)$$

where β_{min} is the minimum ratio of sinus radius to tissue cylinder radius for which oxygen becomes depleted for a given cellular architecture. After rearranging, Eq. 18 becomes

$$\phi = \frac{2}{\sqrt{(\beta_{\text{min}}^2 - 1) - 2 \ln \beta_{\text{min}}}} \quad (19)$$

We are also interested in determining cellular architectures whereby oxygen depletion might occur, where there is no prior information about the size of the tissue cylinder R_2 . Equation 19 cannot be directly used for this purpose because both ϕ and β depend on R_2 . This difficulty can be overcome by multiplying both sides of Eq. 19 with β_{min} to obtain

$$\phi' = \frac{2\beta_{\text{min}}}{\sqrt{(\beta_{\text{min}}^2 - 1) - 2 \ln \beta_{\text{min}}}} \quad (20)$$

where

$$\phi' = R_1 \sqrt{\frac{Q_{\text{max}}}{K \cdot P_s}} \quad (21)$$

For a particular ϕ' , one can solve Eq. 20 to obtain β_{min} .

PARAMETER ESTIMATION

Model parameters are summarized in Table 1 and can be classified into two groups. System parameters define the overall framework of the tissue cylinder and change with the characteristics of the sinus and the cellular arrangement of the hematopoietic tissue. Cellular parameters describe oxygen transport and consumption characteristics of various cell types. Because cellular properties vary with the lineage and differentiation stage of hematopoietic cells, a range of values (Table 2) is considered in most cases to establish possible oxygen-limited situations. Five distinct hematopoietic cell types—erythrocytes, lymphocytes, granulocytes, megakaryocytes, and monocytes—and adipocytes are considered in our model.

System parameters

Sinuses are ~ 10 – $60 \mu\text{m}$ in diameter, which is larger than arteriole (~ 10 – $30 \mu\text{m}$) and venule (12 – $20 \mu\text{m}$) diameters

TABLE 2 Summary of cellular parameters of individual cell types in the bone marrow hematopoietic compartment. Note symbols are shown after the parameter value(s)

	Granulocytes	Monocytes	Lymphocytes	Erythrocytes	Megakaryocytes	Adipocytes
Fraction of cells (without adipocytes) (as %)	16.9–100*	0–4.3*	2.5–25*	3.46–37.6*	0–3*†	0‡
Cell diameter (μm)	10–25§	12–50§	9–20¶	6.7–8§	30–160§	50–300
Average cell diameter (μm)	17.5	31.0	14.5	7.35	95.0	175.0
Specific cell volume × 10 ⁹ (cm ³ /cell)	2.8	15.6	1.6	0.208	448.9	2806
Specific oxygen uptake rate × 10 ¹⁴ (mol/cell/h)	2.2–64.9**	2.2–64.9††	0.07–5.0‡‡	0.162–0.649§§	144¶¶	32.4
Volumetric oxygen consumption rate × 10 ⁹ (mol/cm ³ /s)	2.2–64.4	0.4–11.6	0.1–7.1	2.2–8.7	0.89	0.03
Effective oxygen permeability × 10 ¹⁴ (mol/cm/s/mm Hg)	3.20***	3.20***	2.99***	1.58†††	3.54***	9.11***
Effective oxygen diffusion coefficient × 10 ⁵ (cm ² /s)	1.58***	1.58***	1.63***	0.90†††	1.52***	1.57***

*Custer, 1974; McDonald et al., 1988; Platt, 1979.

†Wickramasinghe, 1975.

‡Fraction of cells is estimated based on hematopoietic marrow only.

§Heilmeyer and Begemann, 1989; McDonald et al., 1988; Wickramasinghe, 1975.

¶Custer, 1974; Heilmeyer and Begemann, 1989; McDonald et al., 1988.

||Marshall and Lichtman, 1981.

**Calculated from Bird et al., 1951, and Collins et al., 1998.

††Monocytes are assumed to have oxygen metabolism similar to granulocytes.

‡‡Guzman Barron and Harrop, 1929.

§§Calculated from Bishop and Surgenor, 1964.

¶¶Calculated from Grunewald and Sowa, 1977, and Wintrobe, 1961.

|||Bottcher et al., 1995.

***Values are estimated using Riley's correlation (Riley et al., 1996) and methods suggested by Dutta and Popel (1995).

†††Experimental data and literature values (Bishop and Surgenor, 1964; Goldstick et al., 1975) instead of the calculated values are used for further calculations due to the presence of hemoglobin, which was not accounted for in our estimation.

(Lightfoot, 1973; Tavassoli and Yoffey, 1983). For our models, the sinus radius is conservatively taken to be 5 μm. The radius of the tissue cylinder (R_2) is estimated from the cellular distance between two neighboring sinuses, which corresponds to ~4–20 cell diameters (Erslev and Weiss, 1983; Lichtman, 1984; Weiss, 1976). Another estimate of the tissue cylinder radius is the size of a lymphocyte nodule (80–1200 μm in diameter located between two sinuses), in which lymphocytes are organized in the human BMHC (Wickramasinghe, 1975). Our model is used to evaluate the effects of changes in R_2 on pO₂ distribution. Oxygen tension at the sinus wall is expected to be intermediate between those in arteries (95 mm Hg) and veins (40 mm Hg). A reported mean pO₂ in healthy adult BM is 52 mm Hg (Ishikawa and Ito, 1988). Because oxygen diffuses from the sinus to the extravascular hematopoietic tissue, pO₂ at the sinus wall (P_S) should be higher than 52 mm Hg. We used $P_S = 52$ mm Hg for our models as a conservative value for estimating possible oxygen depletion.

Cellular parameters

Differential cell count data from the literature provide a range of fractions of individual cell types in the BM (Table 2). Similarly, cell diameters of various types of hematopoietic cells were collected from the literature and combined to estimate the upper and lower bounds of cell diameters. Average cell diameters were used in our calculations. Erythrocytes are the smallest and adipocytes are the largest among all cell types. Megakaryocytes and adipocytes show

much larger variations in size than leukocytes and erythrocytes.

The specific oxygen consumption rate (q_{O_2}) of granulocytes and monocytes is 2.2×10^{-14} to 6.49×10^{-13} mol/cell/h (Bird et al., 1951; Collins et al., 1998), while that of human peripheral lymphocytes ranges from 7×10^{-16} to 5×10^{-14} mol/cell/h (Guzman Barron and Harrop, 1929; Hedeskov and Esmann, 1966; Loos and Roos, 1973). Bishop and Surgenor (1964) reported that q_{O_2} values of mature erythrocytes and erythroid progenitors are ~400 and 100 times lower, respectively, than those of leukocytes. The oxygen consumption of megakaryocytes was reported to be as high as that of resting muscle cells (Wintrobe, 1961) (0.1 ml O₂/100 g tissue/min; Grunewald and Sowa, 1977). Using the density of muscle tissue (1.2 g/cm³) and the approximated volume of megakaryocytes (4.49×10^{-7} cm³/cell), we obtained 1.44×10^{-12} mol/cell/h as an estimate for the q_{O_2} value of megakaryocytes. Bottcher et al. (1995) reported that cultured white adipose tissues consume 3.24×10^{-13} mol oxygen/cell/h, which we considered as an upper limit for the q_{O_2} value of marrow adipocytes, because they are metabolically less active in vivo (Bathija et al., 1979; Tavassoli, 1974). Michaelis-Menten kinetics describes the dependence of oxygen uptake rate on pO₂ for a wide range of cell types (Popel, 1989). The K_M value of hematopoietic cells should fall in the reported range of other human cells (0.17–5.9 mm Hg) (Gnaiger et al., 1995), and it has been suggested to be ~1.5–7.6 mm Hg (Peng and Palsson, 1996). Thus, using 1–5% of P_S as K_M , we found that the pO₂

TABLE 3 Oxygen permeability and solubility values for cellular components at 37.4°C. Note symbols are shown after the parameter value

	Permeability (mol/ cm/s/mm Hg)	Solubility (mol/ cm ³ /mm Hg)	Diffusion Coefficient (cm ² /s)
Water	4.67×10^{-14} *	1.42×10^{-9} *	3.29×10^{-5} *
Cytosol	2.80×10^{-14} †	1.76×10^{-9} ‡	1.59×10^{-5} §
Lipid	9.28×10^{-14} *	6.23×10^{-9} *	1.49×10^{-5} *

*Dutta and Popel (1995).

†Darnell et al. (1986).

‡Value is 1.24 times the solubility of water at 22.8°C (Dutta and Popel, 1995).

§The cytosol is assumed to be 70% water and 30% proteins.

profiles were fairly similar to those using the zero-order kinetics (differences were <5%; data not shown).

Hematopoietic cells are closely packed in the marrow with the interstitial space filled with extracellular matrix. Oxygen transport parameters of the extravascular tissue are estimated as tissue layers embedded with different types of cells. The transport of oxygen through the cells and interstitial space is considered separately. For oxygen diffusion through cells, the effective oxygen permeability of hematopoietic cells can be approximated based on the composition of their cellular components. Dutta and Popel (1995) suggested three different methods to compute oxygen permeabilities, assuming cellular components are arranged in a parallel, series, or random manner (Stroevé, 1977). We estimated oxygen permeability using the oxygen transfer parameters of lipid and cytosol (Table 3) and the lipid composition of hematopoietic cells found in the literature (Table 4). As there is no unique way to estimate the effective oxygen permeability, we have taken an average of the values calculated using all three methods (Dutta and Popel, 1995) (Table 4). The results from these calculations indicate that the permeabilities of all cell types are similar with the exception of adipocytes, where the permeability is three times higher than for the other cell types.

The resistance to oxygen diffusion of extracellular matrix, which usually constitutes 10% of total tissue volume, can be approximated by the oxygen permeability of physiological salt solutions (lower than water) (Guyton, 1977). Once oxygen transport parameters of different hematopoietic cells and interstitial tissue are obtained, composite effective oxygen permeabilities of extravascular hematopoietic tissue can be calculated using Riley's correlation (Riley et al., 1996), which was developed for diffusivity of immobilized cell systems. This correlation indicates that the composite effective parameter is a weighed average of the cellular and extracellular parameters. The K values among different cell types are very similar, with the exception of adipocytes and erythrocytes (Table 2).

TABLE 4 Lipid content of hematopoietic cells and estimated K values of hematopoietic cells using three methods described by Dutta and Popel (1995). Note symbols are shown after the parameter value

Cell Type	Lipid Content (% Dry Cell Weight)	Permeability (mol/cm/s/mm Hg) $\times 10^{14}$			
		Parallel**	Series**	Stroevé's ^{††}	Average
Granulocyte	7.3%*	3.27	2.95	3.17	3.13
Monocyte	7.3%†	3.27	2.95	3.17	3.13
Lymphocyte	2.6%‡	2.97	2.85	2.93	2.92
Erythrocyte	1.3%§	2.88	2.83	2.86	2.86
Megakaryocyte	15%¶	3.77	3.13	3.57	3.49
Adipocyte	~100%	9.28	9.28	9.28	9.28

*The calculated dry cell weight of a granulocyte is 296 pg and the lipid concentration is 21.5 pg/cell (Gottfried, 1967).

†The lipid compositions of monocytes and granulocytes are assumed to be similar.

‡The calculated dry cell weight of a lymphocyte is 435 pg and the lipid concentration is 11.1 pg/cell (Gottfried, 1967).

§Wintrobe, 1961.

¶We assumed that human megakaryocytes and platelets have similar lipid compositions (Marcus et al., 1969; Wintrobe, 1961).

||Guyton, 1977.

**Dutta and Popel, 1995.

††Stroevé, 1977.

RESULTS

Granulocytic progenitors result in the largest pO_2 gradients

To examine the most severely oxygen-limited cases based on actual BM physiology, we considered cellular architectures made up of granulocytes because they are the most abundant cell type in the BM (Table 2). Hematopoietic cell metabolism in culture generally peaks at the progenitor stage, and then decreases as the cells mature. To evaluate a range of pO_2 distributions we considered the maximum and minimum q_{O_2} values of granulocytes for progenitors and mature cells, respectively. Simulated oxygen profiles of tissue cylinders with different numbers of layers of granulocytic progenitors and mature granulocytes are shown in Fig. 2, A and B, respectively. In general, pO_2 in the extravascular tissue would decrease and pO_2 gradients would increase with an increasing Thiele modulus ϕ . As the ratio of the sinus radius to tissue cylinder radius β decreases, the pO_2 levels in the extravascular tissue decrease considerably. An increase in the number of cell layers (or tissue cylinder radius) causes a concomitant decrease in β and increase in ϕ . Therefore, oxygen availability in the one-layer tissue cylinder is the highest and the corresponding pO_2 gradient is the smallest among all tissue cylinders (Fig. 2 A). Calculated oxygen tensions at the rim of tissue cylinders (P_{R2}^*), which are occupied by granulocytic progenitors, indicate that oxygen depletion would occur when the number of cell layers is larger than two (Fig. 2 A).

Fig. 2 B represents the pO_2 profiles of tissue cylinders occupied by different numbers of layers of mature granulo-

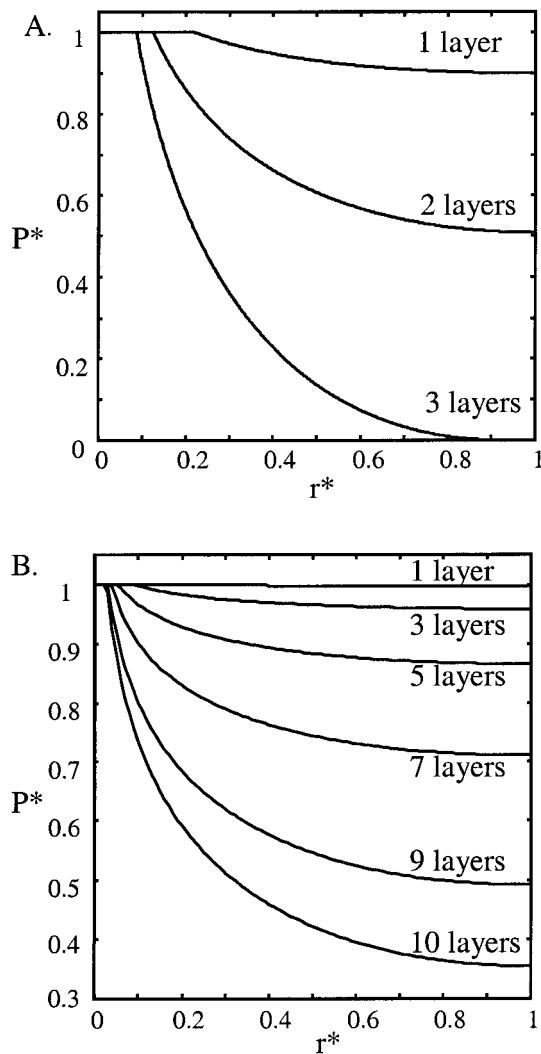


FIGURE 2 Simulated oxygen profiles for (A) granulocytic progenitors ($R_1 = 5 \mu\text{m}$) and (B) mature granulocytes ($R_1 = 5 \mu\text{m}$) using the homogeneous Kroghian model. Selected values for β and ϕ are shown in Table 5. Note that when oxygen depletion occurs, the solution (Eq. 17) to the continuity equation is no longer valid and Eq. A4 of the Appendix should be used instead.

cytes. Because the specific oxygen uptake rate of mature granulocytes is much lower than for granulocytic progenitors (ϕ is smaller), pO₂ levels are generally higher and changes in pO₂ throughout the extravascular tissue are smaller. Oxygen depletion would not occur in an extravascular tissue of mature granulocytes, even if the thickness was as great as 10 cell diameters (Table 5).

Prediction of oxygen depletion

The occurrence of oxygen depletion in the extravascular tissue can be predicted from the maximum tissue cylinder radius $R_{2\text{max}}$ that can be supported by a sinus in a certain cellular architecture. Instead of individually simulating pO₂

TABLE 5 Dimensionless oxygen tensions at the outer boundary of tissue cylinders (P_{R2}^*) occupied by mature and immature granulocytes ($K = 3.20 \times 10^{-14} \text{ mol/cm/s/mm Hg}$, $d = 17.5 \mu\text{m}$, $P_s = 52 \text{ mm Hg}$, and $R_1 = 5 \mu\text{m}$)

	β	ϕ	P_{R2}^*
One-layer ($R_2 = 22.5 \mu\text{m}$)			
Mature ($q_{O_2} = 2.2 \times 10^{-14} \text{ mol/cell/h}$)	0.222	0.081	1
Progenitor ($q_{O_2} = 6.49 \times 10^{-13} \text{ mol/cell/h}$)	0.222	0.442	0.9
Five-layer ($R_2 = 92.5 \mu\text{m}$)			
Mature ($q_{O_2} = 2.2 \times 10^{-14} \text{ mol/cell/h}$)	0.0541	0.335	0.86
Progenitor ($q_{O_2} = 6.49 \times 10^{-13} \text{ mol/cell/h}$)	0.0541	1.817	0
10-layer ($R_2 = 180 \mu\text{m}$)			
Mature ($q_{O_2} = 2.2 \times 10^{-14} \text{ mol/cell/h}$)	0.0278	0.651	0.35
Progenitor ($q_{O_2} = 6.49 \times 10^{-13} \text{ mol/cell/h}$)	0.0278	3.536	0

distribution for tissue cylinders with different numbers of cell layers, one can readily calculate this value from a plot of β_{min} versus ϕ' (Fig. 3). In most cellular architectures considered, the ϕ' values range from 0.001 to 0.1. In this range, β_{min} is almost directly proportional to ϕ' . The value of $R_{2\text{min}}$ can be obtained by dividing the sinus radius R_1 by β_{min} . If β for a particular cellular architecture is smaller than β_{min} , then oxygen depletion will occur.

Different hematopoietic cell types result in distinct pO₂ distributions

Oxygen tension distribution in the local BM environment varies considerably with the type of cells occupying the extravascular tissue. Based on the properties of hematopoietic cells and the characteristics of a sinus, we calculated the modified Thiele modulus ϕ' , from which we estimated the β_{min} value using Eq. 20 (Fig. 3). The maximum tissue cylinder radii ($R_{2\text{max}}$) for granulocytes, monocytes, lymphocytes, erythrocytes, megakaryocytes, and adipocytes that can be supported by a BM sinus of $5 \mu\text{m}$ are shown in Table 6. Among all cases considered the $R_{2\text{max}}$ value of granulo-

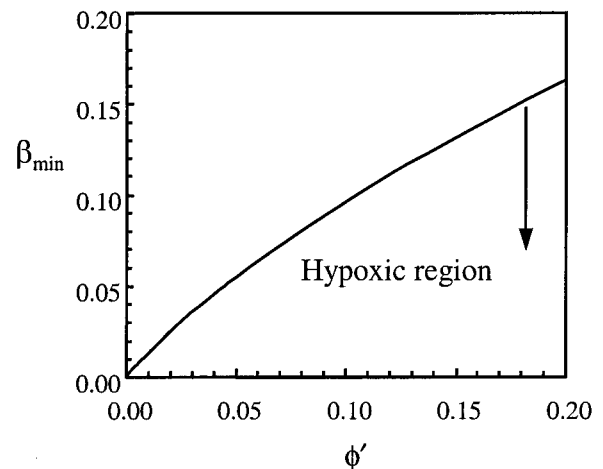


FIGURE 3 β_{min} for various ϕ' values as determined from Eq. 20.

TABLE 6 Maximum tissue cylinder radii and maximum numbers of cell layers for various hematopoietic cells ($P_s = 52$ mm Hg and $R_1 = 5$ μ m)

	ϕ'	β_{\min}	$R_{2\max}$	N_{\max}
Granulocytes ($K = 3.20 \times 10^{-14}$ mol/cm/s/mm Hg; $d = 17.5$ μ m)				
Mature ($q_{O_2} = 2.2 \times 10^{-14}$)*	0.018	0.023	217 μ m	12.1
Progenitor ($q_{O_2} = 6.49 \times 10^{-13}$)*	0.098	0.094	53 μ m	2.7
Monocytes ($K = 3.20 \times 10^{-14}$ mol/cm/s/mm Hg; $d = 31.0$ μ m)				
Mature ($q_{O_2} = 2.2 \times 10^{-14}$)*	7.78×10^{-3}	0.011	454 μ m	14.5
Progenitor ($q_{O_2} = 6.49 \times 10^{-13}$)*	0.042	0.047	106 μ m	3.3
Lymphocytes ($K = 2.99 \times 10^{-14}$ mol/cm/s/mm Hg; $d = 14.5$ μ m)				
Mature ($q_{O_2} = 7.0 \times 10^{-16}$)*	4.35×10^{-3}	6.5×10^{-3}	769 μ m	52.7
Progenitor ($q_{O_2} = 5.0 \times 10^{-14}$)*	0.037	0.043	117 μ m	7.7
Erythrocytes ($K = 1.58 \times 10^{-14}$ mol/cm/s/mm Hg; $d = 7.4$ μ m)				
Mature ($q_{O_2} = 1.62 \times 10^{-15}$)*	0.025	0.031	162 μ m	21.2
Progenitor ($q_{O_2} = 6.49 \times 10^{-15}$)*	0.051	0.056	90 μ m	11.5
Megakaryocytes ($K = 3.54 \times 10^{-14}$ mol/cm/s/mm Hg; $d = 95.0$ μ m)				
Mature ($q_{O_2} = 1.44 \times 10^{-12}$)*	0.011	0.015	335 μ m	3.5
Adipocytes ($K = 9.11 \times 10^{-14}$ mol/cm/s/mm Hg; $d = 175.0$ μ m)				
Mature ($q_{O_2} = 3.24 \times 10^{-13}$)*	1.32×10^{-3}	2.2×10^{-3}	2268 μ m	13.0

*Units of q_{O_2} : mol/cell/h. q_{O_2} generally peaks at the progenitor stage and then decreases as the cells mature. Maximum and minimum reported q_{O_2} values for each lineage have been assigned to progenitor and mature cells, respectively.

cytic progenitors is the smallest, while that of adipocytes is the highest. The maximum number of cell layers that can be supported by a BM sinus (N_{\max}) is also the smallest for the case of granulocytic progenitors. This indicates that granulocytic progenitors indeed result in the most severe pO_2 gradients among all cellular configurations in the homogeneous Kroghian model based on the biophysical data collected.

DISCUSSION

Severe oxygen limitations

Based on biophysical data of the most metabolically active hematopoietic cells and the most abundant cell types in the bone marrow, we have investigated the scenario for the most severe oxygen limitation in the BMHC by constructing a tissue cylinder solely occupied by granulocytic progenitors. Although the possible cellular arrangements are numerous, the actual pO_2 distribution in the extravascular hematopoietic tissue should fall between the pO_2 profiles of adipocytes (the lowest ϕ value) and granulocytic progenitors (the highest ϕ value) (Table 6). Using a mathematical criterion developed from the homogeneous solution of the Kroghian model, we verified that the greatest pO_2 gradients occur in a tissue cylinder solely occupied by granulocytic progenitors.

Estimation of model parameters

Specific oxygen uptake rates (q_{O_2}) for most hematopoietic cells have not been reported in the literature, and among the ones reported, most were measured using old oxygen sensing techniques (Bishop and Surgenor, 1964; Guzman Bar-

ron and Harrop, 1929; Hedeskov and Esmann, 1966; Loos and Roos, 1973). In addition, the majority of these data were collected for a composite cell population without clearly identifying the cellular subgroups present. Also, the oxygen uptake rates measured in culture can be significantly different from those in vivo. The work from our group indicates that the q_{O_2} values for erythroid progenitors should be considerably higher than those estimated by Bishop and Surgenor (1964), and can be as high as those of the granulocytic and monocytic lineages (Collins et al., 1998). However, without further experimental measurements, the original estimates were used so that the effect of a wider range of q_{O_2} on the pO_2 profiles could be examined. The dependence of oxygen consumption on pO_2 was assumed to follow zero-order kinetics in all oxygen models developed. From simulations of pO_2 distribution using Michaelis-Menten kinetics and various K_M values, we found that K_M did not affect the pO_2 distribution significantly unless oxygen was depleted (data not shown).

Cell volume also contributes considerably to variations in oxygen availability. For the same q_{O_2} value, the overall pO_2 levels in a tissue cylinder solely occupied by small hematopoietic cells (Table 2) are always lower than those in tissue cylinders filled with cells of a larger diameter. Thus, the maximum tissue cylinder radius without oxygen depletion decreases when the volume of hematopoietic cells is reduced.

In general, compared to other model parameters, oxygen permeability (K) has a small influence on pO_2 distributions in the extravascular tissue, primarily due to the much smaller range of K values. As oxygen permeabilities of most hematopoietic cells have not been reported in the literature, we estimated K values by considering the contribution of

both hematopoietic cells and extracellular matrix to the resistance of oxygen diffusion in the tissue. The estimates of cellular oxygen permeability obtained from three different methods were fairly similar in their magnitudes (Table 4). The oxygen permeabilities of most hematopoietic cells except erythrocytes were also similar (Table 2). For adipocytes, the oxygen permeability is only three times higher than that of granulocytes and monocytes, even though their lipid compositions differ by ~14-fold.

Oxygen tension at the sinus wall (P_s) is another factor affecting oxygen supply to the surrounding tissue. Changes in P_s result in different ϕ values, and the corresponding dimensionless oxygen profiles vary as well. However, when the reduced parameters are converted back to their dimensional form, these changes do not alter the actual gradient of the pO₂ profiles. For example, an increase in P_s only causes an upward shift in overall pO₂ profiles. This is because variations in P_s only alter the boundary condition at the sinus, while the boundary condition at the rim of the tissue cylinder remains the same.

Model versus cellular complexity

We chose the Kroghian model over other mathematical frameworks because it is a widely accepted one (Grunewald and Sowa, 1977). The original Kroghian model deals only with homogeneous muscular tissue surrounding a capillary. However, hematopoietic tissue in the BMHC is quite different due to the complexity of cellular architectures and the heterogeneity in cell types. In reality, hematopoietic cells of different types can be found in close proximity to one another, which we fail to address in our current model. To approximate this physiological feature one should use composite cellular properties or consider an additional spatial dimension in the oxygen transport model. Modifications have been made to the Kroghian model to handle these differences, and these are discussed in the companion paper.

APPENDIX

When oxygen depletion occurs, Eq. 17 cannot describe the oxygen distribution in the BMHC because $R_2 > R_{2\max}$. The value of $R_{2\max}$ can be obtained by dividing R_1 by β_{\min} , which is estimated from Fig. 3 at a particular ϕ' (calculated using Eq. 20). In the case of three layers of granulocytic progenitors, R_2 and $R_{2\max}$ are 57.5 μm and 52.74 μm , respectively ($\phi' = 0.0983$ and $\beta_{\min} = 0.0948$). The oxygen distribution in the region where $r > R_{2\max}$ is zero. For the region $R_1 < r \leq R_{2\max}$, the boundary value problem is described by Eq. 2 with boundary conditions given by Eq. 3 and

$$\frac{dP}{dr} = 0 \quad \text{when} \quad r = R_{2\max} \quad (\text{A1})$$

Similar to Eq. 17, the solution to this modified boundary value problem is

$$P = P_s + \frac{Q_{\max}}{K} \left[\frac{r^2 - R_1^2}{4} + \frac{R_{2\max}^2}{2} \ln\left(\frac{R_1}{r}\right) \right] \quad (\text{A2})$$

To compare this profile with the previously developed solution (Eq. 17), we rewrite Eq. A2 as

$$P^* = 1 + \frac{R_2^2 \cdot Q_{\max}}{P_s \cdot K} \left[\frac{(r/R_2)^2 - (R_1/R_2)^2}{4} + \frac{1}{2} \cdot \frac{R_{2\max}^2}{R_2^2} \ln\left(\frac{R_1/R_2}{r/R_2}\right) \right] \quad (\text{A3})$$

$$P^* = 1 + \phi^2 \left[\frac{r^{*2} - \beta^2}{4} + \frac{1}{2} \left(\frac{R_{2\max}}{R_2} \right)^2 \ln\left(\frac{\beta}{r^*}\right) \right] \quad (\text{A4})$$

This work was supported by National Institutes of Health Grant R01HL48276.

REFERENCES

- Adler, S. S. 1984. Blood circulation of bone marrow. *In* Blood Vessels and Lymphatics in Organ Systems. D. E. Abramson and R. B. Dobrin, editors. Academic Press, San Diego. 705–719.
- Bathija, A., S. David, and S. Trubowitz. 1979. Bone marrow adipose tissue: response to starvation. *Am. J. Hematol.* 6:191–198.
- Bird, R. M., J. A. Clements, and L. M. Becker. 1951. The metabolism of leukocytes taken from peripheral blood of leukemic patients. *Cancer.* 4:1009–1014.
- Bishop, C., and D. M. Surgenor. 1964. The Red Blood Cell: a Comprehensive Treatise. Academic Press, New York.
- Bottcher, H., S. Engel, and P. Furst. 1995. Determination of gaseous and dissolved oxygen in a closed fat cell culture system. *Anal. Biochem.* 230:149–153.
- Bradley, T. R., G. S. Hodgson, and M. Rosendaal. 1978. The effect of oxygen tension on haemopoietic and fibroblast cell proliferation in vitro. *J. Cell. Physiol.* 97(3 Pt. 2 Suppl. 1):517–522.
- Brizel, D. M., R. K. Dodge, R. W. Clough, and M. W. Dewhirst. 1999. Oxygenation of head and neck cancer: changes during radiotherapy and impact on treatment outcome. *Radiother. Oncol.* 53:113–117.
- Carmeliet, P., and R. K. Jain. 2000. Angiogenesis in cancer and other diseases. *Nature.* 407:249–257.
- Collins, P. C., L. K. Nielsen, S. D. Patel, E. T. Papoutsakis, and W. M. Miller. 1998. Characterization of hematopoietic cell expansion, oxygen uptake, and glycolysis in a controlled, stirred-tank bioreactor system. *Biotechnol. Prog.* 14:466–472.
- Custer, R. P. 1974. An Atlas of the Blood and Bone Marrow, 2nd Ed. W. B. Saunders Company, Philadelphia.
- Darnell, J. E., H. F. Lodish, and D. Baltimore. 1986. Molecular Cell Biology. W. H. Freeman, New York.
- Dutta, A., and A. S. Popel. 1995. A theoretical analysis of intracellular oxygen diffusion. *J. Theor. Biol.* 176:433–435.
- Erslev, A. J., and L. Weiss. 1983. Structure and function of the marrow. *In* Hematology, 12th Ed. W. J. Williams, E. Beutler, A. J. Erslev, and M. A. Lichtman, editors. McGraw-Hill, New York. 75–83.
- Gnaiger, E., R. Steinlechner-Maran, G. Mendex, T. Eberl, and R. Margreiter. 1995. Control of mitochondrial and cellular respiration by oxygen. *J. Bioenerg. Biomembr.* 27:583–596.
- Goldstick, T. K., V. T. Ciuryla, and L. Zucherman. 1975. Diffusion of oxygen in plasma and blood. *In* Oxygen Transport to Tissue II, 1st Ed. J. Grote, D. Reneau, and G. Thews, editors. Plenum Press, New York.
- Gottfried, E. L. 1967. Lipids of human leukocytes: relation to cell type. *J. Lipid Res.* 8:321–327.
- Grossmann, U. 1982. Simulation of combined transfer of oxygen and heat through the skin using a capillary loop model. *Math. Biosci.* 61:205–236.

- Grunewald, W. A., and W. Sowa. 1977. Capillary structures and O₂ supply to tissue: an analysis with a digital diffusion model as applied to the skeletal muscle. *Rev. Physiol. Biochem. Pharmacol.* 77:205–212.
- Grunewald, W. A., and W. Sowa. 1978. Distribution of the myocardial tissue PO₂ in the rat and the inhomogeneity of the coronary bed. *Pflugers Arch.* 374:57–66.
- Guyton, A. C. 1977. Basic Human Physiology: Normal Function and Mechanics of Disease. W. B. Saunders Company, Philadelphia.
- Guzman Barron, E. S., and G. A. Harrop, Jr. 1929. Studies on blood cell metabolism. *J. Biol. Chem.* 84:89–100.
- Hansen-Algenstaedt, N., B. R. Stoll, T. P. Padera, D. E. Dolmans, D. J. Hicklin, D. Fukumura, and R. K. Jain. 2000. Tumor oxygenation in hormone-dependent tumors during vascular endothelial growth factor receptor-2 blockade, hormone ablation, and chemotherapy. *Cancer Res.* 60:4556–4560.
- Hedekov, C. J., and V. Esmann. 1966. Respiration and glycolysis of normal human lymphocytes. *Blood.* 28:163–174.
- Heilmeyer, L., and H. Begemann. 1989. Atlas of Clinical Hematology. Springer-Verlag, New York.
- Helminger, G., F. Yuan, M. Dellian, and R. K. Jain. 1997. Interstitial pH and pO₂ gradients in solid tumors in vivo: high-resolution measurements reveal a lack of correlation. *Nature Med.* 3:177–182.
- Hevehan, L. H., E. T. Papoutsakis, and W. M. Miller. 2000. Physiologically significant effects of pH and oxygen tension on granulopoiesis. *Exp. Hematol.* 28:267–275.
- Hoofd, L., Z. Turek, and K. Rakusan. 1987. Diffusion pathways in oxygen supply of cardiac muscle. *Adv. Exp. Med. Biol.* 215:171–177.
- Ishikawa, Y., and T. Ito. 1988. Kinetics of hematopoietic stem cells in a hypoxic culture. *Eur. J. Haematol.* 40:126–129.
- Ivanov, K. P., Y. Y. Kislyakov, and M. O. Samoilov. 1979. Microcirculation and transport of oxygen to neurons of the brain. *Microvasc. Res.* 18:434–441.
- Katahira, J., and H. Mizoguchi. 1987. Improvement of culture conditions for human megakaryocytic and pluripotent progenitor cells by low oxygen tension. *Int. J. Cell Cloning.* 5:412–420.
- Koller, M. K., J. G. Bender, E. T. Papoutsakis, and W. M. Miller. 1992. Reduced oxygen tension increases hematopoiesis in long-term culture of human stem and progenitor cells from the cord blood and bone marrow. *Exp. Hematol.* 20:264–270.
- Krogh, A. 1918. The rate of diffusion of gases through animal tissue with some remarks on the coefficient of invasion. *J. Physiol. (Lond.).* 52:391–409.
- Krogh, A. 1919. The number and distribution of capillaries in muscle with calculations of the oxygen pressure head necessary for supplying the tissue. *J. Physiol. (Lond.).* 52:409–415.
- LaIppa, J. A., E. T. Papoutsakis, and W. M. Miller. 1998. Oxygen tension alters the effects of cytokines on the megakaryocyte, erythrocyte, and granulocyte lineages. *Exp. Hematol.* 26:835–843.
- Leunig, M., F. Yuan, M. D. Menger, Y. Boucher, A. E. Goetz, K. Messmer, and R. K. Jain. 1992. Angiogenesis, microvascular architecture, microhemodynamics, and interstitial fluid pressure during early growth of human adenocarcinoma LS174T in SCID mice. *Cancer Res.* 52:6553–6560.
- Lichtman, M. A. 1984. The relationship of stromal cells to hematopoietic cells in marrow. In Long-Term Bone Marrow Culture, 1st Ed. D. G. Wright and J. S. Greenberger, editors. Alan R. Liss Inc., New York. 3–29.
- Lightfoot, E. N. 1973. Transport Phenomena and Living Systems: Biomedical Aspects of Momentum and Mass Transport. Wiley, New York.
- Loos, J. A., and D. Roos. 1973. Changes in the carbohydrate metabolism of human blood lymphocytes during antigenic stimulation. In Erythrocytes, Thrombocytes, Leukocytes. E. Gerlach, K. Moser, E. Deutsch, and W. Wilmanns, editors. George Thieme Publishers, New York.
- Marcus, A. J., H. L. Ullman, and L. B. Safier. 1969. Lipid composition of subcellular particles of human blood platelets. *J. Lipid Res.* 10:108–114.
- Marshall, A., and M. D. Lichtman. 1981. The ultrastructure of the hematopoietic environment of the marrow: a review. *J. Hematol.* 9:391–410.
- McDonald, G. A., P. James, and B. Cruickshank. 1988. Atlas of Haematology. Churchill Livingstone, New York.
- Mostafa, S. S., W. M. Miller, and E. T. Papoutsakis. 2000. Oxygen tension influences the differentiation, maturation, and apoptosis of human megakaryocytes. *Br. J. Haematol.* 111:879–889.
- Peng, C.-A., and B. O. Palsson. 1996. Determination of specific oxygen uptake rates in human hematopoietic cultures and implications for bioreactor design. *Ann. Biomed. Eng.* 24:373–381.
- Platt, W. R. 1979. Color Atlas and Textbook of Hematology, 2nd Ed. J. B. Lippincott Company, Philadelphia.
- Popel, A. S. 1989. Theory of oxygen transport to tissue. *Crit. Rev. Biomed. Eng.* 17:257–321.
- Rakusan, K. 1971. Oxygen in the Heart Muscle. Charles C Thomas, Springfield, IL.
- Rakusan, K., L. Hoofd, and Z. Turek. 1984. The effect of cell size and capillary spacing on myocardial oxygen supply. *Adv. Exp. Med. Biol.* 180:463–475.
- Reneau, D. D., Jr., D. F. Bruley, and M. H. Knisely. 1967. A mathematical simulation of oxygen release, diffusion, and consumption in the capillaries and tissue of the human brain. In Chemical Engineering in Medicine and Biology. D. Hershey, editor. Plenum Press, New York. 135.
- Riley, M. R., R. J. Muzzio, H. M. Buettner, and S. C. Reyes. 1996. A simple correlation for predicting effective diffusivities in immobilized cell systems. *Biotechnol. Bioeng.* 49:223–227.
- Roh, H. D., Y. Boucher, S. Kalnicki, R. Buchsbaum, W. D. Bloomer, and R. K. Jain. 1991. Interstitial hypertension in carcinoma of uterine cervix in patients: possible correlation with tumor oxygen and radiation response. *Cancer Res.* 51:6695–6698.
- Stroeve, P. 1977. Diffusion with irreversible chemical reaction in heterogeneous media: application to oxygen transport in respiring tissue. *J. Theor. Biol.* 64:237–251.
- Tavassoli, M. 1974. Differential response of bone marrow and extramedullary adipose cells to starvation. *Experientia.* 30:424–425.
- Tavassoli, M. J., and M. Yoffey. 1983. Bone marrow: structure and function. Alan R. Liss Inc., New York.
- Thews, G. 1960. Die Sauerstoffdiffusion im Gehirn. Ein Beitrag zur Frage der Sauerstoffversorgung der Organe. *Pflugers Arch.* 271:197.
- Vaupel, P., and M. Hoeckel. 1999. Predictive power of the tumor oxygenation status. *Adv. Exp. Med. Biol.* 471:533–539.
- Weibel, E. R. 1984. The Pathway for Oxygen: Structure and Function in the Mammalian Respiratory System. Harvard University Press, Cambridge, MA.
- Weiss, L. P. 1976. The hematopoietic microenvironment of the bone marrow: an ultrastructural study of the stroma in rats. *Anat. Rec.* 186:161–184.
- Weiss, L. P. 1991. Functional organization of the hematopoietic tissues. In Hematology: Basic Principles and Practice, 8th Ed. R. Hoffman, E. J. Benz, S. J. Shattil, B. Furie, and H. J. Cohen, editors. Churchill Livingstone, New York. 82–86.
- Wickramasinghe, S. N. 1975. Human Bone Marrow. Blackwell Scientific Publications, Oxford, distributed by J. B. Lippincott, Philadelphia.
- Wintrobe, M. M. 1961. Clinical Hematology, 5th Ed. Lea and Febiger, Philadelphia.